P2H.6 Microphysical and dynamical characteristics in the stratiform region of Tropical Storm Gabrielle at landfall

Dong-Kyun Kim, Kevin R. Knupp, and Christopher Williams[1]

University of Alabama in Huntsville, Huntsville, Alabama
[1]Cooperative Institute for Research in Environmental Sciences, University of Colorado at Boulder
Boulder, Colorado

1. Introduction

Studying the dynamics and microphysics in stratiform regions of tropical storms is significant due to their contribution to total water budget (i.e. condensation and evaporation) (Gamache et al. 1993) since stratiform precipitation accounts for a relatively large fraction of tropical precipitation. As a significant component of deep stratiform structures, the melting layer has been investigated in many observational and numerical studies (Drummond et al. 1996; Fabry and Zawadzki 1995; Huggel et al. 1996; Srivastava 1987; Willis and Heymsfield 1989; Zawadzki et al. 2005). Willis and Heymsfield (1989) noted that the 0°C isothermal layer formed by melting-driven cooling acts like a transition layer that separates dynamics above and below the melting layer. The melting-driven cooling, concentrated in a narrow melting zone, is more significant in producing mesoscale downdrafts than evaporative cooling from raindrops (Srivastava 1987). As most critical to dynamical and microphysical properties within stratiform precipitation, vertical air motion and horizontal divergence are acquired by using the single-Doppler radar techniques such as VAD (Velocity Azimuth Display) (Browning and Wexler 1968) and EVAD (the extended VAD) (Srivastava et al. 1986; Matejka and Srivastava 1991). Melting-driven cooling can affect the change in bright band intensity and height, depending on precipitation content as well as aggregation degree near the top of the melting layer. The vertical variations in raindrop size distributions (RSDs) below the melting layer are closely linked to the bright band characteristics above.

In this study, we utilize the EVAD, the quasi-VAD technique (Q-VAD), and the divergence theorem, and also perform the RSD retrievals and a quantitative parameter analysis in order to understand the melting layer dynamics and microphysics in the stratiform region of Gabrielle.

2. Case

On 12 UTC 14 September 2001 tropical storm Gabrielle made landfall along the west coast of Florida. Detailed observations of Gabrielle were made by Mobile Integrated Profiling Systems (MIPS), a SMART-Radar located 1 km east of the MIPS, and the Tampa Bay WSR-88D (TBW) radar located about 70 km to the north (see Figure 1).

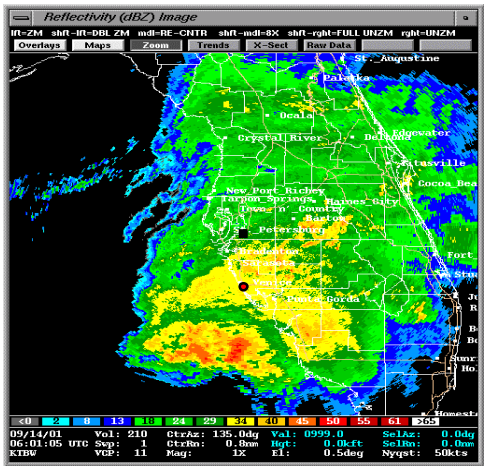

Figure 1. The TBW radar reflectivity image on 0601 UTC (0.5°). The red circle and black rectangle show the locations of MIPS/SMART-Radar and the TBW radar, respectively.

The storm moved north and northeastward at a speed of about 7 m s^{-1}. An extensive region of stratiform precipitation preceded a strong convective region between 0430 and 0700 UTC. Winds were southeasterly at the surface and veered with height. During this period, wind fields were sufficiently uniform to meet the assumption for the EVAD technique. The SMART-Radar (5.5 cm wavelength) has elevation angles from 1.8 to 44.2° incorporating 17 elevation sweeps over a 5 min period. The 915-MHz wind profiler was operated using five beams; one is vertical and four others are off-vertical 23.6 degree from the zenith. The dwell time on each beam is about 30 sec, and the vertical beam was sampled every 60 s. The0600 UTC Tampa Bay sounding indicated the

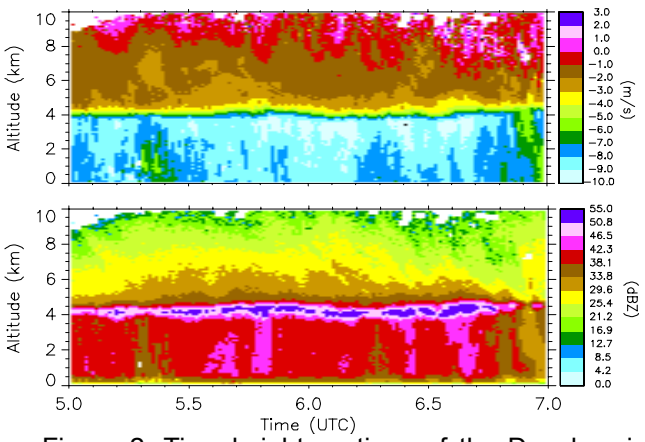

Figure 2. Time-height sections of the Doppler air velocity (top) and reflectivity (bottom) from the 915-MHz profiler on 14 Sep. 2001.

0°C level near 4.7 km. In Figure 2, a pronounced bright band signature was observed by the 915-MHz profiler and the TBW radar between 0500 and 0650 UTC. The bright band height undulated slightly during this time and the notable reflectivity streaks were present below the strong bright band (Figure 2). The profile of reflectivity showed almost constant reflectivity with decreasing height below the melting layer. The rainfall rates showed an abrupt increase (up to 15~20 mm hr^{-1}) especially when the bright band became stronger and thicker.

3. Method

In this study, vertical air motions are obtained from the fallspeed-reflectivity relations for snow and rain above and below the melting layer. Linear interpolation is used for vertical air motions between the snow and rain level. The EVAD and Q-VAD (i.e. the profiler kinematic method) are applied to the SMART-Radar and the 915-MHz profiler, respectively, for examining profiles of horizontal divergence and vertical air motion. In addition, the divergence theorem is applied to the highest elevation angle of the SMART-Radar as a supplement to the Q-VAD divergence profile. A quantitative parameter study is conducted to examine bright band properties using the basic parameters from the snow and rain levels determined at reflectivity maximum curvature, and the gamma parameter ($\gamma=Z_{snow}V_{snow}/Z_{rain}V_{rain}$, Drummond et al. 1996) that also determines the dominance of aggregation or breakup within the melting layer. Lastly, the Sans Air Motion (SAM) model (Williams 2002) is used for retrieving the RSDs and precipitation parameters below the melting layer.

4. Results

In Figure 3, time variations of the γ parameter show that aggregation ($\gamma < 0.23$) occurred during most of the analysis time. Dominant breakup is less frequent and is also likely at around 0530 and 0540 UTC. Relatively stronger downdrafts were observed from 0600 to 0610 UTC. Overall, the both smaller Z_{snow}/Z_{rain} and V_{snow}/V_{rain} during this

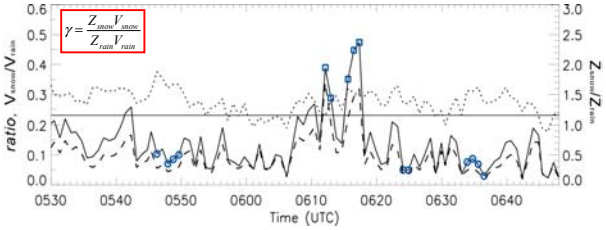

Figure 3. Time variations of the γ parameter (solid line), reflectivity ratio (Z_{snow}/Z_{rain}) (dashed line), and Doppler velocity ratio (dotted line). The rectangle and circle symbols represent the breakup- and aggregation-dominant periods, respectively.

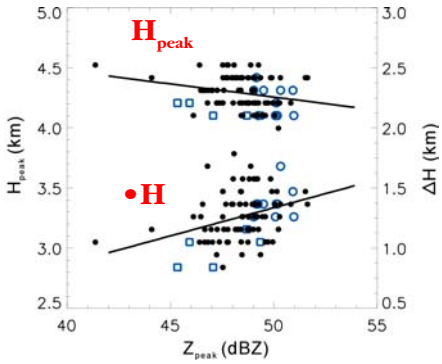

Figure 4. Scatterplot of Z_{peak} versus the bright band height (top, left axis) and thickness (bottom, right axis). The symbols are as defined in Figure 3.

period indicate the presence of smaller aggregates near the top of the melting layer.

As proportional to bright band intensity (i.e. aggregation degree), melting-driven cooling played an important role in propagating the convergence layer downward as well as producing downdrafts near the melting layer. Importantly, the levels of reflectivity maxima dropped (~ 200 m) especially when there were stronger downdrafts. In Figure 4, the reflectivity maxima (Z_{peak}) were inversely proportional to the bright band height (H_{peak}) because of a significant amount of melting-

driven cooling particularly during aggregation-dominant periods, consistent with Durden et al. (1997). Z_{peak} was proportional to the bright band thickness. This is probably due to a longer fall distance for complete melting of large snow aggregates. Bright band intensity was stronger during aggregation-dominant periods as Z_{peak} is proportional to bright band intensity.

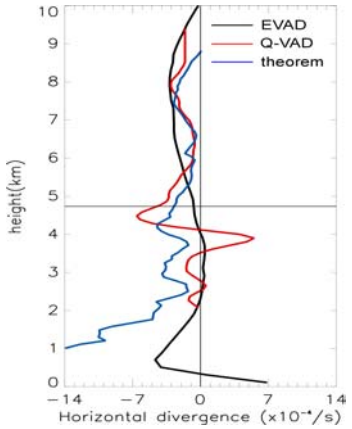

Figure 5. Composite divergence profiles averaged over the 0545-0631 UTC period. The solid line represents the divergence profile from the EVAD, the red line from the Q-VAD, and the blue line from the divergence theorem. The Horizontal line shows the approximate top of the melting layer.

In Figure 5, the divergence profiles from the EVAD, Q-VAD and divergence theorem are in better agreement above the melting layer. However, the discrepancy increases below the melting layer primarily due to the decrease in range (or horizontal distance for the profiler) as well as the difference in sampling volume of the three techniques. One notable feature is that the Q-VAD composite divergence profile shows a distinct and narrow convergence peak near the top of the melting layer and divergence beneath it. Another convergence-divergence couplet from the divergence theorem supports that this couplet is not an artifact but a result of the fine-scale variations of airflow due to cooling and the increased downward accelerations of hydrometeors. It is speculated that a negative heating rate ($\Delta\dot{Q}/\Delta p = \rho^{-1}\nabla \cdot V_H$)(upper side of cooling peak) from a significant amount of cooling is related to convergence whereas a positive $\Delta\dot{Q}/\Delta p$ (lower side of cooling peak) makes it crossover to the divergence just below the convergence due to reduced cold temperature anomaly, that is, relatively increased warm temperature anomaly (Mapes and Houze 1995) due to adiabatic descents.

5. Drop size distributions

By using the SAM, the averaged RSDs at the bottom of the melting layer were retrieved during the four major periods. As shown in Figure 6, there

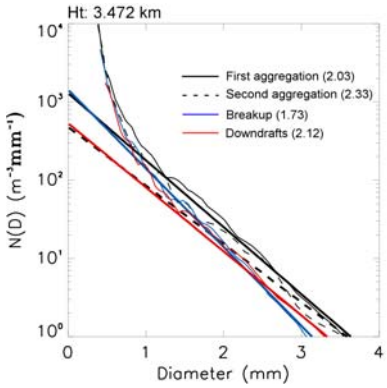

Figure 6. Comparison of the averaged RSDs during the four major periods at 3472 m AGL. The black solid line represents the RSD during the first aggregation-dominant period, the dashed line the RSD during the second aggregation-dominant period, the blue line the RSD during breakup-dominant periods, and the red line the RSD during downdraft periods. The thick lines are those retrieved from the SAM model and the thin lines are those from the measured spectra. The number in bracket indicates the mass-weighted mean diameter (mm).

was comparatively smaller number concentration of smaller drops during the strong downdraft period. The large number of small drops is probably collected by large drops within downdrafts. During the strong downdraft period, there was a slight increase in Z and D_m with decreasing height, indicative of raindrop growth by collection. In addition, drying driven by downdrafts and a relative increase in evaporation would contribute to the low concentrations of small drops. The larger number of large drops during aggregation-dominant periods seems to result from melting of large snow aggregates above the melting layer. While, the larger number of small drops and smaller number of larger drops producing the smallest D_m during breakup-dominant period represents that there would be more effective breakup in the lower part of the melting layer.

6. Conclusions

In this study, the melting layer dynamics and microphysics in a relatively intense stratifrom rainbands of Gabrielle were investigated by using the EVAD, Q-VAD, and divergence theorem, and by performing the melting layer parameter study and the RSD retrievals. Melting-driven cooling is a critical physical process around the melting layer, affecting the bright band intensity and even playing a role on producing the mesoscale downdrafts. The almost constant profile of reflectivity below the melting layer indicates the balance between raindrop growth by collection and breakup/evaporation. It was found that the raindrop growth (i.e. slight increase in Z and D_m) might be possible by collection even within strong downdrafts. The convergence-divergence couplets both derived from the Q-VAD and the divergence theorem strongly suggest that these are a result of the fine-scale airflow variability driven by a significant cooling and a quick downward acceleration of melting hydrometeors around the melting layer. Furthermore, this result recognizes the importance of the wind profiler application into melting layer studies.

It was shown that the RSDs near the bottom of the melting layer have a close connection with snow size distributions near the top of the melting layer. During aggregation-dominant periods, the larger number of large drops is a result from melting of large snow aggregates above the melting layer. In contrast, the larger number of small drops and smaller number of larger drops during breakup-dominant periods represents that breakup is relatively more active in the lower part of the melting layer. This is supported by the fact that Z_{peak}-Z_{bottom} was larger during breakup-dominant periods than during aggregation-dominant periods.

7. References

Browning, K. A., and R. Wexler. 1968: The Determination of Kinematic Properties of a Wind Field Using Doppler Radar. *J. Appl. Meteor.,* **7,** 105–113.

Drummond, F. J., R.R. Rogers, S.A. Cohn, W.L. Ecklund, D.A. Carter, and J.S. Wilson, 1996: A New Look at the Melting Layer. *J. Atmos. Sci.,* **53,** 759–769.

Durden, L. S., A. Kitiyakara, E. Im, A. B. Tanner, Z. S. Haddad, F. K. Li, and W. J. Wilson, 1997: ARMAR Observations of the Melting Layer During TOGA COARE. EEE transactions on geoscience and remote sensing, 35, 6, 1453-1456.

Fabry, F., and I. Zawadzki, 1995: Long-Term Radar Observations of the Melting Layer of Precipitation and Their Interpretation. *J. Atmos. Sci.,* **52,** 838–851.

Gamache, J. K., R. A. Houze Jr., and F. D. Marks Jr., 1993: Dual-Aircraft Investigation of the inner Core of Hurricane Norbert. Part III: Water Budget. *J. Atmos. Sci.,* **50,** 3221–3243.

Huggel, A., W. Schmid, and A. Waldvogel, 1996: Raindrop Size Distributions and the Radar Bright Band. *J. Appl. Meteor.,* **35,** 1688–1701.

Mapes, B., and R. A. Houze, 1995: Diabatic divergence profiles in Western Pacific mesoscale convective systems. *J. Atmos. Sci.,* **52,** 1807-1828.

Matejka, T., and R. C. Srivastava. 1991: An Improved Version of the Extended Velocity-Azimuth Display Analysis of Single-Doppler Radar Data. *J. Atmos. Oceanic Technol.,* **8,** 453–466.

Srivastava, R. C., T.J. Matejka and T.J. Lorello. 1986: Doppler Radar Study of the Trailing Anvil Region Associated with a Squall Line. *J. Atmos. Sci.,* **43,** 356–377.

Srivastava, R. C., 1987: A model of intense downdrafts driven by the melting and evaporation of precipitation. *J. Atmos. Sci.,* **44,** 1752–1773.

Williams, C. R., 2002: Simultaneous ambient air motion and raindrop size distributions retrieved from UHF vertical incident profiler observations. *Radio Sci.,* 37(2), 1024, doi:10.1029/2000RS002603.

Willis, P. T., and A. J. Heymsfield, 1989: Structure of the Melting Layer in Mesoscale Convective System Stratiform Precipitation. *J. Atmos. Sci.,* **46,** 2008–2025.

Zawadzki, I., W. Szyrmer, C. Bell, and F. Fabry, 2005: Modeling of the Melting Layer. Part III: The Density Effect, *J. Atmos. Sci.,* **62,** 3705–3723.